Applied Numerical Mathematics ••• (••••) •••–•••

Contents lists available at ScienceDirect

Applied Numerical Mathematics

www.elsevier.com/locate/apnum

Iterative methods for anisotropic diffusion of speckled medical images

Clovis Tauber [a,b], Pierre Spiteri [c,*], Hadj Batatia [c]

[a] UMRS INSERM U930 – CNRS FRE 2448, Université François Rabelais, 2 boulevard Tonnellé, F-37044 Tours, France
[b] Institut Pasteur, Quantitative Image Analysis Unit, URA CNRS 2582, 25 rue du Docteur Roux, F-75015 Paris Cedex 15, France
[c] IRIT – ENSEEIHT, UMR CNRS 5505, 2 rue Camichel, BP 7122, F-31071 Toulouse Cedex, France

ARTICLE INFO

Article history:
Received 19 May 2008
Received in revised form 9 June 2009
Accepted 6 November 2009
Available online xxxx

Keywords:
Iterative method
Boundary value problem
Large scale system
Relaxation method
Conjugate gradient method
Anisotropic diffusion
Nonlinear filtering
Speckle
Ultrasound imaging

ABSTRACT

This paper deals with filtering multiplicative noise that corrupts ultrasound medical images. The aim is to increase their contrast, while preserving edges and structures. From a mathematical point of view, this requires solving numerically an evolutive nonlinear boundary value problem. Several discretization schemes are studied for the stationary problem as well as for the evolutive problem. The behavior of various iterative methods is analyzed when semi-implicit time marching schemes are used. Results of sequential simulations are presented.

1. Introduction

Due to destructive interferences of signals reflected from scatterers within a single resolution cell, ultrasound medical images are corrupted by a specific multiplicative noise, commonly called speckle. It can alter accuracy of diagnosis; it is therefore necessary to restore the image using an appropriate filter.

In order to achieve this objective, this paper aims at four image processing goals

1) filter out the noise,
2) increase contrast and the quantity of information perceived,
3) preserve edges and structures of information,
4) allow accurate and fast computation of complex and large medical images.

In a previous work [12], we have proposed a robust speckle reducing anisotropic diffusion model which deals with limitations of related works (see [1,4,6,9,17]), such as insufficient noise attenuation, lack of edge preservation, instability and slowness. The proposed model is a nonlinear evolutive boundary value problem of diffusion with homogeneous Neumann boundary condition (see [2]). In the definition of this model, the coefficient of diffusion vanishes locally at some points of the domain Ω where the partial differential equation is defined. This property implies the fact that the discretization matrix can be reducible. The solution of the evolutive boundary value problem can be achieved by various time marching schemes.

* Corresponding author.
E-mail address: Pierre.Spiteri@enseeiht.fr (P. Spiteri).

0168-9274/$30.00 © 2009 Published by Elsevier B.V. on behalf of IMACS.
doi:10.1016/j.apnum.2009.11.002

The use of an explicit scheme can be problematic since such method suffers from stability limitations. Whereas, the use of a fully implicit time marching scheme is problematic as it requires the use of the Newton method due to nonlinearity. In addition, the implementation of the Newton method is difficult in the considered model, since the computation of the derivative of coefficient of diffusion is not easy. Furthermore, the convergence of the Newton method at each time step is not guaranteed in the general case and practical criteria of convergence are not obvious to obtain. This two facts constitute a strong limitation when an implicit time marching scheme is considered to solve the evolutive problem. Another difficulty consists in the fact that, when an implicit or semi-implicit scheme is used, the linear systems to solve at each time step can be ill-conditioned, due to the Neumann boundary condition.

In order to solve numerically this anisotropic diffusion problem, and better take into account its nonlinear part, we propose in the present study two time marching semi-implicit discretization schemes derived from the classical implicit and the Gear implicit schemes (see [7]). These semi-implicit schemes are compared with the classical explicit scheme. The consistency and stability are studied specifically for all the considered schemes.

In the case of semi-implicit and Gear semi-implicit schemes, it is necessary to solve at each time step a large linear system. Due to the size of these systems, iterative methods, such as point relaxation or conjugate gradient methods, are preferred to direct methods. An originality of the present study, specific to image processing, comes from the spatial discretization step size along each direction which is fixed implicitly to a constant value defined by the distance between two consecutive pixels. Commonly, in the literature, the value of the spatial discretization step size is fixed to one (see [9] and [16]). This particularity, inherent only to our knowledge to image processing, involves very particular properties of the numerical parameters, mainly the spectral radius and the condition number, allowing to estimate the asymptotic rate of convergence of point relaxation and conjugate gradient methods. However, despite the Neumann boundary condition, these iterative algorithms have a very high convergence speed. Note that this behavior is ineffective in the physical context of heat conduction equation where the spatial discretization step size can be very small leading to problems hard to solve numerically by the same methods. Precisely, in such a case, the spectral radius of the relaxation matrix is close to one or the condition number leads to infinity.

The remainder of the paper is organized as follows. In Section 2, the mathematical model of the anisotropic diffusion problem is presented. In Section 3, spatial discretization schemes, explicit and semi-implicit discretization time marching schemes are established and analyzed; particularly the consistency and the numerical stability are studied. Section 4 is devoted to the analysis of the behavior of the point relaxation and the conjugate gradient methods; in particular, due to the value of the spatial discretization step size fixed to one, we show why we obtain efficient rate of convergence and why preconditioning is not necessary when conjugate gradient method is used. In the last section, we present the results of numerical simulations, concerning both the quality of image processing as well as the performance of the iterative methods used for solving the linear systems.

2. The mathematical model of anisotropic diffusion

2.1. Ultrasound image processing

Ultrasound imaging is a technique widely used for medical applications. It is non-invasive, real-time and relatively inexpensive. However, compared to other medical imaging techniques, it suffers from low signal to noise ratio, low contrast and the presence of speckle, which appears as a strong granularity within regions that should be homogeneous. The speckle is a multiplicative, locally correlated noise caused by destructive interference of signals reflected from scatterers within one resolution cell. This phenomenon degrades the resolution of images and makes difficult the detection of their features. Therefore, the development of effective noise reduction filters for echographic images is of primary importance in order to enhance the image allowing better diagnosis and facilitating higher level processing like image segmentation, which aims at localizing objects and boundaries, and quantification.

Image filtering techniques aim at reducing the noise while enhancing the perception of important structures. Among these, anisotropic diffusion was proposed by Perona and Malik [9]. It is derived from the physical principle of heat diffusion. A gradient of temperature leads to the heat diffusion from high temperature toward low temperature points tending to a balanced distribution. Similarly, the anisotropic diffusion is used in image processing to diffuse the differences of intensity between adjacent pixels. The goal is to reduce the noise in homogeneous regions. Noise creates variance in the intensity of pixels of homogeneous regions that should otherwise have similar values. The diffusion is anisotropic to preserve edges between regions: on edge pixels, diffusion occurs only along the edge, not across it. The anisotropy derives from the diffusion coefficient denoted in the sequel c, which controls the diffusion process making it isotropic in homogeneous regions, and slow across image contours.

Anisotropic diffusion has been largely studied for filtering additive noise (see [1,6,5,16]). But most of the models proposed in the literature have two inherent limitations: their tendency to produce a totally flat image after a high number of iterations, and their relative ineffectiveness to filter images affected by multiplicative noise, such as speckle.

2.2. The γ-diffusion partial derivative equation

In [12], we proposed an anisotropic diffusion model, called γ-diffusion, which addresses the previous limitations; in a bounded domain $\Omega \subset \mathbb{R}^2$ this model is defined as follows

Please cite this article in press as: C. Tauber et al., Iterative methods for anisotropic diffusion of speckled medical images, Applied Numerical Mathematics (2009), doi:10.1016/j.apnum.2009.11.002

$$\frac{\partial u(x,y,t)}{\partial t} - \operatorname{div}\big(c(x,y,t,u)\nabla u(x,y,t)\big) = 0, \quad \text{everywhere in } \Omega, 0 < t \leqslant T \tag{1}$$

where ∇u stands for the gradient of u. In order to prevent energy from escaping outside the domain Ω, the Neumann boundary condition are set.

The coefficient of diffusion c is derived from the weight function of Tukey [13], applied to the local coefficient of variation denoted $\gamma(x,y,t,u)$ and defined hereafter by (4) (see [12]). The coefficient of diffusion assigns zero weights to outliers having a magnitude above a certain threshold (see [12] and [4]). This allows stopping completely the diffusion in the directions corresponding to high values of the local coefficient of variation

$$c(x,y,t,u) = \begin{cases} \left[1 - \dfrac{\gamma^2(x,y,t,u)}{5\gamma_g^2(u,t)}\right]^2 & \text{if } \gamma(x,y,t,u) \leqslant \sqrt{5}\gamma_g(u,t), \\ 0 & \text{elsewhere,} \end{cases} \tag{2}$$

where γ_g is the global coefficient of variation defined as follows

$$\gamma_g^2(u,t) = \frac{\operatorname{var}(u)}{\bar{u}^2}, \tag{3}$$

where $\operatorname{var}(u)$ and $\bar{u}$ are the variance and the mean of the intensity in a homogeneous reflectivity area. The coefficient γ_g can also be estimated automatically (see [12] and [10]). The local coefficient of variation γ is a local version of the global coefficient of variation, defined as follows

$$\gamma^2(x,y,t,u) = \frac{1}{|\eta_s|}\sum_{P\in\eta_s}\frac{(u(P)-\overline{u_s})^2}{\overline{u_s}^2}, \tag{4}$$

where η_s is a neighborhood of a central pixel s, $\overline{u_s}$ is the mean intensity in η_s and $|\eta_s|$ is the area of η_s. In [12] we established that the local coefficient of variation can be written as the sum of the global coefficient of variation and a positive term that increases with the variance of the real reflectivity of the scene. This means that γ is close to γ_g within homogeneous regions, and largely greater than γ_g on edges. It can thus be used to adapt locally the coefficient of diffusion, allowing the diffusion within homogeneous regions, and progressively slowing it on edges.

3. Discretization schemes

Consider the following model of anisotropic diffusion of speckled images

$$\begin{cases} \dfrac{\partial u(x,y,t)}{\partial t} - \operatorname{div}\big(c\nabla u(x,y,t)\big) = 0, \quad \text{everywhere in } \Omega, 0 < t \leqslant T, \\ \dfrac{\partial u(x,y,t)}{\partial n}_{|\partial\Omega} = 0, \quad \forall t \in [0,T] \quad \text{(boundary condition)}, \\ u(x,y,0) = u_0(x,y) \quad \text{(initial condition)}, \end{cases} \tag{5}$$

where $\Omega = [0,d]\times[0,b]$ is a rectangular domain, $\partial\Omega$ is the boundary of the domain Ω, $u = u(x,y,t)$ is the intensity, T is a strictly positive real number, n is the outward vector normal to $\partial\Omega$ and the nonnegative coefficient of diffusion $c = c(x,y,t,u)$ depends of the intensity u. Note that, for this particular application, we have

$$0 \leqslant c(x,y,t,u) \leqslant 1, \quad \text{everywhere in } \Omega, 0 < t \leqslant T. \tag{6}$$

Note also that the boundary value problem (5) is nonlinear. In order to solve numerically the problem (5), we will construct and analyze in the sequel appropriate discretization schemes.

3.1. Spatial discretization scheme

For the spatial discretization of the operator arising in (5), it is necessary to take into account that the diffusion coefficient is not constant in the domain Ω. Then, the discretization scheme is carried out by taking the mean of two intermediate schemes, called in the sequel forward–backward scheme and backward–forward scheme.

3.1.1. Forward–backward scheme

Consider the approximation of $-\frac{\partial}{\partial x}(c(x_i,y_j)\frac{\partial u(x_i,y_j)}{\partial x})$, in the case where the spatial discretization step, denoted by h in the sequel, is uniform and y_j is fixed. Then, if appropriate assumption of regularity concerning c and u are verified, the forward–backward scheme leads to

Please cite this article in press as: C. Tauber et al., Iterative methods for anisotropic diffusion of speckled medical images, Applied Numerical Mathematics (2009), doi:10.1016/j.apnum.2009.11.002

$$\frac{\partial}{\partial x}\left(c(x_i,y_j)\frac{\partial u(x_i,y_j)}{\partial x}\right)=\frac{1}{h}\left(c(x_{i+1},y_j)\frac{u(x_{i+1},y_j)-u(x_i,y_j)}{h}\right)-\frac{1}{h}\left(c(x_i,y_j)\frac{u(x_i,y_j)-u(x_{i-1},y_j)}{h}\right)+\mathcal{E}_x^f(x_i,y_j),$$

where $\mathcal{E}_x^f(x_i,y_j)$ is the local truncation error given by

$$\mathcal{E}_x^f(x_i,y_j)=-\frac{h}{2}\left(\frac{\partial c(x_i,y_j)}{\partial x}\frac{\partial^2 u(x_i,y_j)}{\partial x^2}+\frac{\partial^2 c(x_i,y_j)}{\partial x^2}\frac{\partial u(x_i,y_j)}{\partial x}\right)+\mathcal{O}\big(h^2\big).$$

3.1.2. Backward–forward scheme

Similarly, when the same properties of c and u hold, the backward–forward scheme leads to

$$\frac{\partial}{\partial x}\left(c(x_i,y_j)\frac{\partial u(x_i,y_j)}{\partial x}\right)=\frac{1}{h}\left(c(x_i,y_j)\frac{u(x_{i+1},y_j)-u(x_i,y_j)}{h}\right)-\frac{1}{h}\left(c(x_{i-1},y_j)\frac{u(x_i,y_j)-u(x_{i-1},y_j)}{h}\right)+\mathcal{E}_x^b(x_i,y_j),$$

where $\mathcal{E}_x^b(x_i,y_j)$ is the corresponding local truncation error given by

$$\mathcal{E}_x^b(x_i,y_j)=\frac{h}{2}\left(\frac{\partial c(x_i,y_j)}{\partial x}\frac{\partial^2 u(x_i,y_j)}{\partial x^2}+\frac{\partial^2 c(x_i,y_j)}{\partial x^2}\frac{\partial u(x_i,y_j)}{\partial x}\right)+\mathcal{O}\big(h^2\big).$$

3.1.3. Final discretization scheme

Then, the final discretization scheme of the considered operator is obtained by taking the mean of the two previous schemes; so we obtain

$$\begin{aligned}\frac{\partial}{\partial x}\left(c(x_i,y_j)\frac{\partial u(x_i,y_j)}{\partial x}\right)=\frac{1}{2h^2}\big(&\big(c(x_{i+1},y_j)+c(x_i,y_j)\big)u(x_{i+1},y_j)\\&-\big(c(x_{i+1},y_j)+2c(x_i,y_j)+c(x_{i-1},y_j)\big)u(x_i,y_j)\\&+\big(c(x_i,y_j)+c(x_{i-1},y_j)\big)u(x_{i-1},y_j)\big)+\mathcal{O}\big(h^2\big).\end{aligned}$$

Similarly, the second partial derivative with respect to y is obtained by using the same procedure, when x_i is fixed; then we obtain

$$\begin{aligned}\frac{\partial}{\partial y}\left(c(x_i,y_j)\frac{\partial u(x_i,y_j)}{\partial y}\right)=\frac{1}{2h^2}\big(&\big(c(x_i,y_{j+1})+c(x_i,y_j)\big)u(x_i,y_{j+1})\\&-\big(c(x_i,y_{j+1})+2c(x_i,y_j)+c(x_i,y_{j-1})\big)u(x_i,y_j)\\&+\big(c(x_i,y_j)+c(x_i,y_{j-1})\big)u(x_{i-1},y_{j-1})\big)+\mathcal{O}\big(h^2\big).\end{aligned}$$

The boundary value problem (5) is usually solved using an implicit or a semi-implicit time marching numerical scheme. To take into account such temporal discretization, we have to perturb the stationary boundary value problem with Neumann boundary condition, associated with problem (5) by δu, where δ is a positive real number. In fact, according to the numerical time marching scheme used, δ is proportional to the inverse of the time step. Then, according to the previous remark, for the two-dimensional elliptic problem, we have to discretize the following stationary problem

$$\begin{cases}-\operatorname{div}\big(c(x,y)\nabla u(x,y)\big)+\delta u(x,y)=0, & \text{everywhere in } \Omega,\\ \dfrac{\partial u(x,y)}{\partial n}_{|\partial\Omega}=0 & \text{(boundary condition)},\end{cases}$$

instead of the differential operator $-\operatorname{div}(c(x,y)\nabla u(x,y))$. Thus, for the two-dimensional elliptic problem,

$$\begin{cases}-\dfrac{\partial}{\partial x}\left(c(x,y)\dfrac{\partial u}{\partial x}\right)-\dfrac{\partial}{\partial y}\left(c(x,y)\dfrac{\partial u}{\partial y}\right)+\delta u(x,y)=f(x,y), & \text{in }]0,a[\times]0,b[,\ \delta>0,\\ \dfrac{\partial u(x,y)}{\partial n}_{|\partial\Omega}=0,\end{cases}\tag{7}$$

we can derive a global scheme from the two previous discretization approximations of the two considered operators. For sake of simplicity, we also denote by $c_{i,j}$ for all i and j the value of $c(x_i,y_j)$. According to the size of the image to process, we also denote by $n+2$ and $m+2$, respectively the number of pixels on $[0,d]$ and $[0,b]$, respectively. Assume for example, that the grid points are numbered line by line in a natural ordering from left to right; assume also that the inner grid points

of coordinates $x_i = ih, 1 \leqslant i \leqslant n$, and $y_j = jh, 1 \leqslant j \leqslant m$, are labelled by an index l defined according to the considered ordering, by $l = (i-1)n + j$. Then, by combining the two previous final schemes obtained in each direction, we can set the following scheme associated to the inner grid points

$$-\bar{a}_{l,l-n}u_{l-n} - \bar{a}_{l,l-1}u_{l-1} + (\bar{a}_{l,l} + \delta)u_l - \bar{a}_{l,l+1}u_{l+1} - \bar{a}_{l,l+n}u_{l+n} = f_l, \quad 1 \leqslant l \leqslant nm,$$

where for $1 \leqslant i \leqslant n$ and $1 \leqslant j \leqslant m$, $u_l \equiv u_{i,j}$; then the absolute value of the off-diagonal entries of the matrix are given by

$$\bar{a}_{l,l-n} = \frac{(c_{i,j} + c_{i-1,j})}{2h^2} \quad \text{and} \quad \bar{a}_{l,l+n} = \frac{(c_{i,j} + c_{i+1,j})}{2h^2},$$
$$\bar{a}_{l,l-1} = \frac{(c_{i,j} + c_{i,j-1})}{2h^2} \quad \text{and} \quad \bar{a}_{l,l+1} = \frac{(c_{i,j} + c_{i,j+1})}{2h^2},$$

and the diagonal ones are defined by

$$\bar{a}_{l,l} = \frac{(c_{i-1,j} + 2c_{i,j} + c_{i+1,j})}{2h^2} + \frac{(c_{i,j-1} + 2c_{i,j} + c_{i,j+1})}{2h^2}.$$

Note also that, due to the Neumann boundary condition, for the grid points near the boundary $\partial\Omega$, the above scheme can be obviously simplified in a straightforward way by taking into account that the value of the intensity at this grid point is equal to the value of the intensity at the next grid nodes which belongs to $\partial\Omega$. Let us denote by $\bar{A}$ the discretization matrix with entries $\bar{a}_{l,j}$. Then, it can be verified that the discretization matrix $\bar{A}$ is symmetric with strictly positive diagonal entries and nonpositive off-diagonal entries. Thus, the matrix A, defined by $A = 2h^2\bar{A}$, has the same properties. Moreover, the matrix $(\delta I + \frac{1}{2h^2}A)$, where I is the identity matrix, is symmetric and strictly diagonally dominant, with strictly positive diagonal entries. Consequently, $(\delta I + \frac{1}{2h^2}A)$ is symmetric positive definite and, obviously is a Stieltjes matrix (or symmetric M-matrix) (see [14]). Moreover the local truncation error for the approximation is given by $\mathcal{O}(h^2)$ and the resulting spatial discretization scheme is of order two and is consequently consistent.

3.2. Explicit discretization scheme for the anisotropic diffusion problem

In this subsection, we draw up an appropriate explicit discretization scheme for the nonlinear boundary value problem (5), by taking into account the scheme obtained in Section 3.1. Let us write now the problem (5) for $t_k = k\tau, k \in \mathbb{N}$, where τ denotes the time step; then, we can write

$$\frac{\partial u(x,y,t_k)}{\partial t} - \frac{\partial}{\partial x}\left(c\big(x,y,t_k,u^{(k)}\big)\frac{\partial u(x,y,t_k)}{\partial x}\right) - \frac{\partial}{\partial y}\left(c\big(x,y,t_k,u^{(k)}\big)\frac{\partial u(x,y,t_k)}{\partial y}\right) = 0,$$

where $u^{(k)}$ corresponds to the value of u when $t = t_k$. Let $\alpha = \frac{\tau}{2h^2}$; note that, for the particular application concerning image processing, the spatial discretization step size h is here mentioned for memory; in fact in image processing, the spatial discretization step size along each direction is defined implicitly by the distance between two pixels and can be fixed so that $h = h_x = h_y$; practically, h is fixed to the value one (see [9] and [16]). In the sequel, we will see that the value of h has no effect with respect to the behavior of the studied algorithms since the spatial step size is non-dimensional. Denote also by $U^{(k)}$ the vector of components $u_l^{(k)}, 1 \leqslant l \leqslant nm$, approximation of $u(x_i, y_j, t_k)$. In the sequel $U^{(0)}$ is given by the components $u_0(x_i, y_j)$ of the initial condition arising in (5). Then, classically, the explicit scheme is given by

$$U^{(k+1)} = \big(I - \alpha A^{(k)}\big)U^{(k)}, \quad k = 0, 1, \ldots. \tag{8}$$

Entries of the matrix $A^{(k)}$ are defined in a similar way than the entries of the matrix A in Section 3.1; in fact this matrix $A^{(k)}$ represents the spatial discretization matrix defined at step k of the problem (5) in which the coefficients $c_{i,j}$ are replaced by $c_{i,j}^{(k)}$ with $c_{i,j}^{(k)} = c(x_i, y_j, t_k, u_{i,j}^{(k)})$. Then, we have immediately the following results.

Proposition 1. *Assume that the diffusion coefficient c and the intensity u are continuous and sufficiently differentiable. Then, the explicit scheme* (8) *is consistent and the local truncation error of the scheme denoted by* $E_{i,j}^{(k)}$ *verifies* $|E_{i,j}^{(k)}| \leqslant \mathcal{C}(\tau + h^2)$, *where* $\mathcal{C}$ *is a constant.*

Proof. The result is obviously an immediate consequence of the fact that the explicit scheme (8) is of order one with respect to the time and of order two with respect to the space. □

Remark 1. Note that, except for edges where the diffusion coefficient vanishes, images are mostly constituted of homogeneous regions where the coefficient of variation is relatively smooth. So, diffusion coefficient is also smooth and the previous discretization scheme is based on realistic framework.

Please cite this article in press as: C. Tauber et al., Iterative methods for anisotropic diffusion of speckled medical images, Applied Numerical Mathematics (2009), doi:10.1016/j.apnum.2009.11.002

Proposition 2. *Denote by $\lambda_l^{(k)}, l = 1, \ldots, nm$, the eigenvalues of the spatial discretization matrix at each time step k. Denote also by $\lambda_M^{(k)}$ the greatest eigenvalue of the matrix $A^{(k)}$ at each step k. If the following condition $\alpha < \frac{2}{\lambda_M^{(k)}}$ is verified, then the explicit scheme* (8) *is stable.*

Proof. Note that, at each time step k, the discretization matrix $A^{(k)}$ is symmetric. Then $A^{(k)}$ is diagonalizable and the eigenvalues of the matrix $(I - \alpha A^{(k)})$ are equal to $\mu_l^{(k)} = 1 - \alpha\lambda_l^{(k)}$. Thus obviously, the explicit scheme (8) is stable if $-1 < 1 - \alpha\lambda_l^{(k)} < 1$; so the expected condition leads by taking the more restrictive bound, which achieves the proof. □

Corollary 1. *Denote by $\|A^{(k)}\|$ every norm of the matrix $A^{(k)}$. If the time step size verifies for each $k \in \mathbb{N}$*

$$\tau < \frac{4h^2}{\|A^{(k)}\|},$$

then the explicit scheme (8) *is stable. Particularly, if we consider the case where the norm of the matrix $A^{(k)}$ is induced by the uniform norm or by the l_1-norm, respectively, and if we denote by $\|A^{(k)}\|_\infty$ or by $\|A^{(k)}\|_1$, respectively, the corresponding particular matrix norm, then the previous condition can be written as follows*

$$\tau < \frac{4h^2}{\max\limits_{1\leqslant i\leqslant nm}\left(\sum\limits_{j=1}^{nm}|a_{i,j}^{(k)}|\right)} = \frac{4h^2}{\max\limits_{1\leqslant j\leqslant nm}\left(\sum\limits_{i=1}^{nm}|a_{i,j}^{(k)}|\right)}. \tag{9}$$

Proof. Recall that, for every norm we have $\lambda_M^{(k)} \leqslant \|A^{(k)}\|, \forall k \in \mathbb{N}$. Then, when $\lambda_M^{(k)} = \|A^{(k)}\|$ the first condition follows from a straightforward way from Proposition 2. Since the discretization matrix is symmetric

$$\left\|A^{(k)}\right\|_\infty = \max_{1\leqslant i\leqslant nm}\left(\sum_{j=1}^{nm}|a_{i,j}^{(k)}|\right) \quad \text{and} \quad \left\|A^{(k)}\right\|_1 = \max_{1\leqslant j\leqslant nm}\left(\sum_{i=1}^{nm}|a_{i,j}^{(k)}|\right);$$

then $\|A^{(k)}\|_\infty = \|A^{(k)}\|_1$, which achieves the proof. □

Remark 2. In the case where the differential operator is the classical Laplacian multiplied by c, where c denotes here the constant diffusion coefficient, then the discretization matrix A is such that

$$\sum_{j=1}^{nm}|a_{i,j}| = 8, \quad \text{for all } i \in \{1, \ldots, nm\};$$

then the previous condition (9) is $\tau < \frac{h^2}{4c}$. This previous bound is consistent with both bounds for this classical problem and with the result of Proposition 2.

3.3. Semi-implicit discretization scheme for the anisotropic diffusion problem

Due to the stability condition, and particularly the fact that this condition implies that the time step τ must be small, one likes better use fully-implicit time marching scheme; in our case, such fully-implicit scheme is defined by

$$\left(I + \alpha A^{(k+1)}\right)U^{(k+1)} = U^{(k)}, \quad k = 0, 1, \ldots.$$

Due to the nonlinearity, particularly the definition of the diffusion coefficient, the previous algebraic system can be hard to solve. If the Newton method is used, the derivative of the diffusion coefficient with respect to the components of the intensity, can be hard to obtain, due to the definition of the diffusion coefficient. Moreover, the solution of the fully-implicit scheme can be more complicated to solve and the iterative methods, like the Newton method, do not necessarily converge. It is the reason why, for image processing, the following semi-implicit time marching scheme

$$\left(\theta I + \alpha A^{(k)}\right)U^{(k+1)} = U^{(k)}, \quad k = 0, 1, \ldots,$$

is preferred. In this scheme, θ can take the two values 1 or $\frac{3}{2}$ corresponding to the following situations

$$\theta = \begin{cases} 1 & \text{for the use of the semi-implicit scheme,} \\ \dfrac{3}{2} & \text{for the use of the Gear semi-implicit scheme.} \end{cases} \tag{10}$$

More precisely the semi-implicit scheme is defined as follows

$$\left(I+\alpha A^{(k)}\right)U^{(k+1)}=U^{(k)},\quad k=0,1,\ldots, \tag{11}$$

and corresponds to a time marching scheme with two levels k and $k+1$, while the Gear semi-implicit scheme corresponds to a scheme with three levels $k-1, k$ and $k+1$ and satisfies

$$\left(\frac{3}{2}I+\alpha A^{(k)}\right)U^{(k+1)}=2U^{(k)}-\frac{1}{2}U^{(k-1)},\quad k=1,\ldots; \tag{12}$$

note that it is necessary to initialize the Gear semi-implicit scheme, for example, with the semi-implicit scheme or the explicit scheme. Concerning the numerical analysis of the behavior of the two semi-implicit time marching schemes, we have the following result.

Proposition 3. *Assume that the diffusion coefficient c and the intensity u are continuous and sufficiently differentiable. Then, the semi-implicit schemes* (11) *and* (12) *are unconditionally stable. Moreover,*

1) *the semi-implicit scheme* (11) *is consistent and the local truncation error of the scheme denoted by* $(E^{si}_{i,j})^{(k)}$ *verifies* $|(E^{si}_{i,j})^{(k)}|\leqslant \mathcal{C}^{si}(\tau+h^2)$, *where* $\mathcal{C}^{si}$ *is a constant,*
2) *the semi-implicit Gear scheme* (12) *is consistent and the local truncation error of the scheme denoted by* $(E^{ge}_{i,j})^{(k)}$ *verifies* $|(E^{ge}_{i,j})^{(k)}|\leqslant \mathcal{C}^{ge}(\tau^2+h^2)$, *where* $\mathcal{C}^{ge}$ *is a constant.*

Proof. The proof follows from a straightforward adaptation from the one considered to prove similar result in the case of the classical heat conduction equation (see for example [7]). □

Remark 3. Clearly, it follows from the result of the Proposition 3 that unlike the explicit scheme (8), the semi-implicit schemes (11) and (12) do not suffer from any time step size restriction and can be fully adapted to the desired accuracy without the need to choose small time steps for stability reasons. Moreover, note that Remark 1 holds again here.

4. Sequential iterative methods for image processing

In the previous Section 3.3, we have shown that the semi-linearization and the discretization of the anisotropic diffusion problem leads to the solution of a large scale linear algebraic system. The real number θ being defined by (10), the matrix $\mathcal{A}^{(k)}=(\theta I+\alpha A^{(k)})$ is a regular matrix, since at each time step $k\in\mathbb{N}$ it was verified that the matrix $\mathcal{A}^{(k)}$, arising in the linear system to solve, is symmetric positive definite. Moreover, since the algebraic system to solve is a large scale system, iterative methods are numerically more appropriate. From a general point of view concerning the iterative sequential method we have the following result.

Proposition 4. *The matrix defined by* $\mathcal{A}^{(k)}=(\theta I+\alpha A^{(k)})$, $\forall k\in\mathbb{N}$, *is an M-matrix.*

Proof. Since θ is positive, the matrix $\mathcal{A}^{(k)}$ is strictly diagonally dominant; furthermore the diagonal entries of $\mathcal{A}^{(k)}$ are strictly positive and the off-diagonal entries are nonpositive. Then $\mathcal{A}^{(k)}$ is an M-matrix. □

Remark 4. Note that due to the value of the diffusion coefficient, all the coefficients of the same row (or possibly of several rows) of the matrix $A^{(k)}$ can be equal to zero. Then, the matrix $A^{(k)}$ and consequently the matrix $\mathcal{A}^{(k)}$ is not necessarily irreducible. Nevertheless, due to the strict diagonal dominance, $\mathcal{A}^{(k)}$ is invertible.

The result of Proposition 4 is interesting for the study of the behavior of the iterative method, particularly regarding the convergence of such methods. Recall the following result:

Proposition 5. *Let* $\mathcal{A}^{(k)}$ *be a nonsingular M-matrix where* $\mathcal{A}^{(k)}=\mathcal{C}^{(k)}-\mathcal{R}^{(k)}$ *is a splitting of* $\mathcal{A}^{(k)}$ *such that* $\mathcal{G}^{(k)}=(\mathcal{C}^{(k)})^{-1}\mathcal{R}^{(k)}$ *is a nonnegative matrix. Then* $\rho(\mathcal{G}^{(k)})<1$, *where* $\rho(\mathcal{G}^{(k)})$ *is the spectral radius of the matrix* $\mathcal{G}^{(k)}$ *i.e.* $\mathcal{A}^{(k)}=\mathcal{C}^{(k)}-\mathcal{R}^{(k)}$ *is a convergent splitting.*

The reader is referred to the literature, in particular to [3] for a proof of this classical result. Nevertheless, from a practical point of view, it is interesting to obtain sharp estimates of the spectral radius of the iteration matrix, previously denoted $\mathcal{G}^{(k)}$ in Proposition 5. When possible, the obtainment of such estimates can help the user to choose efficiently sequential iterative methods for image processing.

We first consider the point relaxation method and we begin by the point Jacobi method. According to the previous notations, at each time step $k\in\mathbb{N}$ we can write $A^{(k)}=D^{(k)}-(L^{(k)}+(L^{(k)})^T)$, where $D^{(k)}$ is the diagonal part of $A^{(k)}$ and $L^{(k)}$ is the strictly lower triangular part of the matrix $A^{(k)}$. Denote by $\mathcal{D}^{(k)}=\alpha D^{(k)}+\theta I$ and $\mathcal{J}^{(k)}$ the Jacobi's matrix

Please cite this article in press as: C. Tauber et al., Iterative methods for anisotropic diffusion of speckled medical images, Applied Numerical Mathematics (2009), doi:10.1016/j.apnum.2009.11.002

associated to the matrix $\mathcal{A}^{(k)} = (\theta I + \alpha A^{(k)})$. Then $\mathcal{J}^{(k)} = \alpha(\mathcal{D}^{(k)})^{-1}(L^{(k)} + (L^{(k)})^T)$. The spectral radius $\rho^{(k)}$ of the matrix $\mathcal{J}^{(k)}$ verifies $\rho^{(k)} \leqslant \|\mathcal{J}^{(k)}\|_\infty$. Since

$$\sum_{j\neq l}\left(a_{l,j}^{(k)}\right) \leqslant a_{l,l}^{(k)}, \quad \forall l \in [1, nm] \quad \text{and} \quad \forall k \in \mathbb{N},$$

then the matrix $(\alpha D^{(k)} + \theta I)^{-1} D^{(k)}$ being a diagonal matrix, the spectral radius $\rho^{(k)} = \rho(\mathcal{J}^{(k)})$ verifies

$$\rho^{(k)} = \rho\left(\alpha\left(\mathcal{D}^{(k)}\right)^{-1}\left(L^{(k)} + \left(L^{(k)}\right)^T\right)\right) \leqslant \max_{1\leqslant l\leqslant nm}\left(\frac{\alpha\sum_{j\neq l} a_{l,j}^{(k)}}{\alpha a_{l,l}^{(k)} + \theta}\right) \leqslant \max_{1\leqslant l\leqslant nm}\left(\frac{\alpha a_{l,l}^{(k)}}{\alpha a_{l,l}^{(k)} + \theta}\right).$$

Note that $\rho^{(k)} < 1$. Consider the mapping $\phi : s \to \phi(s) = \frac{\alpha s}{\alpha s+\theta}$. The derivative of the mapping ϕ with respect to the variable s is given by $\phi'(s) = \frac{\alpha\theta}{(\alpha s+\theta)^2} > 0$. So the mapping ϕ is strictly isotone and

$$\rho^{(k)} \leqslant \frac{\alpha \max\limits_{1\leqslant l\leqslant nm}(a_{l,l}^{(k)})}{\alpha \max\limits_{1\leqslant l\leqslant nm}(a_{l,l}^{(k)}) + \theta} < 1.$$

Due to (6), the diffusion coefficient is such that $0 \leqslant c \leqslant 1$, and then $\max\limits_{1\leqslant l\leqslant nm}(a_{l,l}^{(k)}) \leqslant 8$; thus

$$\rho^{(k)} \leqslant \hat{\rho} = \frac{8\alpha}{8\alpha + \theta} = \frac{4\tau}{4\tau + \theta} < 1. \tag{13}$$

Since the derivative with respect to τ of the mapping $\psi : \tau \to \psi(\tau) = \frac{4\tau}{4\tau+\theta}$ is equal to $\psi'(\tau) = (\frac{4\tau}{4\tau+\theta})' = \frac{4\theta}{(\theta+4\tau)^2}$, then this derivative is strictly positive and $\rho^{(k)}$ is a strictly isotone mapping with respect to τ.

Remark 5. The previous estimate $\hat{\rho}$ of the spectral radius $\rho^{(k)}$ of the Jacobi matrix is global at each time step k. Note that the matrix $A^{(k)}$ changes during the time marching process. Consequently, the corresponding value of $\rho^{(k)}$, may also change at each time step $k \in \mathbb{N}$. Then a sharper bound of $\rho^{(k)}$ can be obtained by using the classical inequality

$$\rho^{(k)} \leqslant \left\|\mathcal{J}^{(k)}\right\|, \quad \forall k \in \mathbb{N},$$

where $\|\mathcal{J}^{(k)}\|$ denotes the matrix norm of the Jacobi matrix at each step k. In order to obtain an accurate estimation of $\rho^{(k)}$ with the minimum computational cost, it is recommended to use for the norm of $\|\mathcal{J}^{(k)}\|$ the one induced by the uniform vector norm or by the l_1 vector norm. Then, using the uniform vector norm, since $\mathcal{J}^{(k)}$ is a nonnegative matrix, we obtain

$$\rho^{(k)} \leqslant \max_{1\leqslant i\leqslant nm}\left(\sum_{j=1}^{nm}\mathcal{J}_{i,j}^{(k)}\right).$$

Note that we obtain a similar result when using the l_1 vector norm; consequently the estimate of $\rho^{(k)}$ is very easy.

Remark 6. For sake of clarity, consider that the matrix $A^{(k)}$ is the sum of two matrices $A_x^{(k)}$ and $A_y^{(k)}$, where each previous matrix corresponds to the discretization of the differential operators with respect to x and y, respectively. Consider also that the spatial step size h_x and h_y are different in each direction x and y and are defined respectively by $h_x = \frac{d}{n+1}$ and $h_y = \frac{b}{m+1}$, where d and b, respectively, are the length and the width, respectively, of the domain Ω. Denote by $\alpha_x = \frac{\tau}{2}\frac{(n+1)^2}{d^2} = \frac{\tau}{2}\frac{1}{h_x^2}$, and $\alpha_y = \frac{\tau}{2}\frac{(m+1)^2}{b^2} = \frac{\tau}{2}\frac{1}{h_y^2}$. With the previous notations, we can write

$$\mathcal{J}^{(k)} = \left(\theta I + \alpha_x D_x^{(k)} + \alpha_y D_y^{(k)}\right)^{-1}\left(\alpha_x\left(L_x^{(k)} + (L_x^{(k)})^T\right) + \alpha_y\left(L_y^{(k)} + \left(L_y^{(k)}\right)^T\right)\right),$$

where $A_x^{(k)} = D_x^{(k)} - L_x^{(k)} - (L_x^{(k)})^T$ and similarly for $A_y^{(k)}$. Since the sum of the absolute values of the off-diagonal entries of both matrices $A_x^{(k)}$ and $A_y^{(k)}$ are less or equal to the corresponding diagonal entries $(a_x)_{l,l}$ and $(a_y)_{l,l}$, then the spectral radius $\rho^{(k)}$ of the Jacobi matrix $\mathcal{J}^{(k)}$ satisfies

$$\rho^{(k)} \leqslant \frac{\alpha_x(a_x)_{l,l} + \alpha_y(a_y)_{l,l}}{\theta + \alpha_x(a_x)_{l,l} + \alpha_y(a_y)_{l,l}}.$$

Let $X = \frac{(a_x)_{l,l}}{h_x^2}$ and $Y = \frac{(a_y)_{l,l}}{h_y^2}$; then

$$\rho^{(k)} \leqslant \frac{\tau}{2}\frac{X+Y}{\theta + \frac{\tau}{2}(X+Y)}.$$

Table 1
Bounds of spectral radius of the Jacobi and Gauss–Seidel matrices.

τ	Semi-implicit method		Semi-implicit Gear method	
	Jacobi	Gauss–Seidel	Jacobi	Gauss–Seidel
$\frac{1}{5}$	0.44444	0.19753	0.34782	0.12098
$\frac{1}{7}$	0.36363	0.13223	0.27586	0.07609
$\frac{1}{10}$	0.28571	0.08163	0.21052	0.04432
$\frac{1}{20}$	0.16666	0.02777	0.11764	0.01384

Moreover, since the diffusion coefficient is bounded by one, we have obviously $(a_x)_{l,l} \leqslant 4$ and $(a_y)_{l,l} \leqslant 4$; then

$$\rho^{(k)} \leqslant \hat{\rho} = 2\tau \frac{\frac{(n+1)^2}{d^2} + \frac{(m+1)^2}{b^2}}{\theta + 2\tau(\frac{(n+1)^2}{d^2} + \frac{(m+1)^2}{b^2})} < 1 - \epsilon,$$

where ϵ is a small positive real number. In fact, the number n and m being in the general case sufficiently large, from a numerical point of view only, we can see that $\rho^{(k)}$ has a value close to one. Nevertheless, in image processing, recall that one considers that the parameters are non-dimensional such that $n+1 \simeq d$ and $m+1 \simeq b$, and, consequently the spatial discretization step size satisfies $h_x = h_y \approx 1$ (see [9] and [15]); so the upper bound $\hat{\rho}$ of the number $\rho^{(k)}$ is well given by (13) and, since τ is small, the upper bound of $\rho^{(k)}$ is small.

Classically, note that we can deduce from the estimate of the spectral radius of the Jacobi matrix, the asymptotic rate of convergence of the point Jacobi's method, denoted by $R_\infty(\mathcal{J}^{(k)})$ and defined by

$$R_\infty\big(\mathcal{J}^{(k)}\big) = -Ln\big(\rho^{(k)}\big).$$

Consider now the use of the point Gauss–Seidel method for the iterative solution of the algebraic system derived from the discretization of the anisotropic diffusion problem by the semi-implicit time marching scheme. The study of the sequential Gauss–Seidel algorithm is easier thanks to the analysis of the behavior of the sequential Jacobi method. Indeed, if $\rho(\mathcal{GS}^{(k)})$ denotes the spectral radius of the iteration matrix associated to the Gauss–Seidel method, then, classically, we have $\rho(\mathcal{GS}^{(k)}) = (\rho(\mathcal{J}^{(k)}))^2$; using the above obtained estimates we have

$$\rho\big(\mathcal{GS}^{(k)}\big) \leqslant \left(\frac{\alpha \max\limits_{1\leqslant l\leqslant nm}(a_{l,l}^{(k)})}{\alpha \max\limits_{1\leqslant l\leqslant nm}(a_{l,l}^{(k)}) + \theta}\right)^2 < 1,$$

and the corresponding asymptotic rate of convergence of the point Gauss–Seidel's method, denoted by $R_\infty(\mathcal{GS}^{(k)})$ obviously verifies $R_\infty(\mathcal{GS}^{(k)}) = 2R_\infty(\mathcal{J}^{(k)})$; so the Gauss–Seidel method is twice faster than the Jacobi method. We summarize hereafter in Table 1 some values of the spectral radius of the point Jacobi matrix and of the point Gauss–Seidel matrix, for different values of τ, in both cases of semi-implicit and Gear semi-implicit time marching schemes.

Concerning the behavior of the point successive over relaxation method, classically, by the Frankel and Young theory, we know that the optimal relaxation parameter is given by

$$\omega_{opt}^{(k)} = \frac{2}{1 + \sqrt{1 - (\rho(\mathcal{J}^{(k)}))^2}}. \tag{14}$$

Using the previous estimate $\hat{\rho}$ of $\rho^{(k)}$, let us estimate an appropriate value $\hat{\omega}_{opt}$ of $\omega_{opt}^{(k)}$. Since $\rho^{(k)} \simeq \hat{\rho} = \frac{4\tau}{4\tau+\theta}$, then $1 - (\rho^{(k)})^2 \simeq \frac{\theta(\theta+8\tau)}{(\theta+4\tau)^2}$. Thus, as $\sqrt{\theta(\theta+8\tau)} = \theta(1+\frac{8\tau}{\theta})^{\frac{1}{2}}$, then $\sqrt{\theta(\theta+8\tau)} \simeq \theta(1+\frac{4\tau}{\theta}) = (\theta+4\tau)$. Thus, an estimate $\hat{\omega}_{opt}$ of $\omega_{opt}^{(k)}$ is given by $\hat{\omega}_{opt} \approx 1$. In fact, the previous estimate of $\omega_{opt}^{(k)}$ can be slightly improved by considering few additional terms in the Taylor's formula of $\sqrt{\theta(\theta+8\tau)}$. We can write

$$\left(1 + \frac{8\tau}{\theta}\right)^{\frac{1}{2}} \simeq 1 + \frac{4\tau}{\theta} - \frac{8\tau^2}{\theta^2},$$

and then

$$\omega_{opt}^{(k)} \simeq \hat{\omega}_{opt} = \frac{2}{2 - \frac{8\tau^2}{\theta(\theta+4\tau)}} > 1.$$

Note that since $\hat{\rho} \geqslant \rho^{(k)}$, then $1 + \sqrt{1-(\rho^{(k)})^2} \geqslant 1 + \sqrt{1-\hat{\rho}^2}$ and finally $\hat{\omega}_{opt}$ is an over estimation of $\omega_{opt}^{(k)}$.

Please cite this article in press as: C. Tauber et al., Iterative methods for anisotropic diffusion of speckled medical images, Applied Numerical Mathematics (2009), doi:10.1016/j.apnum.2009.11.002

Table 2
Upper bounds of the condition number for semi-implicit and semi-implicit Gear methods.

τ	Semi-implicit	Semi-implicit Gear $\hat{\kappa}_1$	Semi-implicit Gear $\hat{\kappa}_2$
$\frac{1}{5}$	2.60	3.10	2.06
$\frac{1}{7}$	2.14	2.64	1.76
$\frac{1}{10}$	1.80	2.30	1.53
$\frac{1}{20}$	1.40	1.90	1.26

Remark 7. Among the iterative relaxation methods, the block relaxation methods such as the block Jacobi method or the block Gauss–Seidel method and the block successive over-relaxation method are suitable for the solution of the linear system derived from the anisotropic diffusion problem at each time step $k \in \mathbb{N}$. Generally, this kind of block iterative relaxation method has also a good asymptotic rate of convergence, particularly the block successive over-relaxation associated to the optimal relaxation parameter $\bar{\omega}_{opt}$. However, contrary to the classical case, i.e. for the solution of the heat conduction equation, where for example the diagonal entries of the spatial discretization matrix are equal to 4 and the off-diagonal entries are equal to -1 or zero, in the considered application of image processing, note that all the entries of the matrix $\mathcal{A}^{(k)} = (\theta I + \alpha A^{(k)})$ are different. Then, for all blocks and at each time step of the block relaxation method, it is necessary to perform a Gaussian elimination or, in the symmetric definite positive case, a Cholesky elimination, which needs a $\mathcal{LU}$ factorization of each block-diagonal matrices. Since all block-diagonal and all right hand sides of each linear subsystems are different, each factorization and each forward and backward substitution are time consuming. Then, even if the block relaxation method converges faster than the point relaxation method, it does not necessarily need less time of computation. Then the use of block relaxation methods for solving by a numerical way the anisotropic diffusion problem seems to be less interesting.

On another side, for solving at each time step $k \in \mathbb{N}$ the linear system derived from the anisotropic diffusion problem, we can also use the classical conjugate gradient method. Classically, we know that the asymptotic rate of convergence of the classical conjugate gradient method is related to the condition number $\kappa^{(k)}$ of the matrix $\mathcal{A}^{(k)} = (\theta I + \alpha A^{(k)})$ as follows

$$R_\infty\big(\mathcal{CG}^{(k)}\big) \leqslant 4\left(\frac{\sqrt{\kappa^{(k)}} - 1}{\sqrt{\kappa^{(k)}} + 1}\right)^2.$$

In order to estimate the efficiency of the classical conjugate gradient method for solving at each time step $k \in \mathbb{N}$ the linear system, it is necessary to estimate the condition number of the matrix $(\theta I + \alpha A^{(k)})$. Recall that when the matrix $\mathcal{A}^{(k)}$ is symmetric, $\kappa^{(k)}$ is given by

$$\kappa^{(k)} = \frac{\theta + \alpha\lambda_{\max}^{(k)}}{\theta + \alpha\lambda_{\min}^{(k)}}.$$

Since $\frac{1}{\theta+\alpha\lambda_{\min}^{(k)}} < 1$, then $\kappa^{(k)} \leqslant \kappa_1^{(k)} = \theta + \alpha\lambda_{\max}^{(k)}$ and we can estimate the condition number by the value $\kappa_1^{(k)}$, which, since α is small, is very close to θ; in such a case, the preconditioning is not necessary. Note also that, since

$$\lambda_{\max}^{(k)} \leqslant \max_{1\leqslant i\leqslant nm}\left(\sum_{j=1}^{nm}\big(\big|a_{ij}^{(k)}\big|\big)\right) \leqslant 16,$$

then, h being fixed to one, we finally obtain

$$\kappa^{(k)} \leqslant \kappa_1^{(k)} = \theta + \alpha\lambda_{\max}^{(k)} \leqslant \hat{\kappa}_1 = \theta + 16\alpha = \theta + 8\tau.$$

Note also that we can obtain a sharper bound of the condition number; indeed since $\frac{1}{\theta+\alpha\lambda_{\min}^{(k)}} < \frac{1}{\theta}$, and $\lambda_{\max}^{(k)} \leqslant 16$ then we obtain

$$\kappa^{(k)} \leqslant \kappa_2^{(k)} = 1 + \frac{\alpha\lambda_{\max}^{(k)}}{\theta} \leqslant \hat{\kappa}_2 = 1 + \frac{8\tau}{\theta} \approx 1, \tag{15}$$

when τ is small. Note, that $\hat{\kappa}_1 = \hat{\kappa}_2$ if $\theta = 1$; if $\theta = \frac{3}{2}$, corresponding to the Gear scheme, then $\hat{\kappa}_2 < \hat{\kappa}_1$.

We summarize hereafter in Table 2 some upper bounds of $\kappa^{(k)}, k \in \mathbb{N}$ for different values of τ.

Remark 8. As previously mentioned, the bounds of the condition number are very close to the number θ. For comparison, consider the numerical solution of the heat diffusion equation with Dirichlet boundary condition; then, the diffusion coefficient c being constant, we have to solve

Please cite this article in press as: C. Tauber et al., Iterative methods for anisotropic diffusion of speckled medical images, Applied Numerical Mathematics (2009), doi:10.1016/j.apnum.2009.11.002

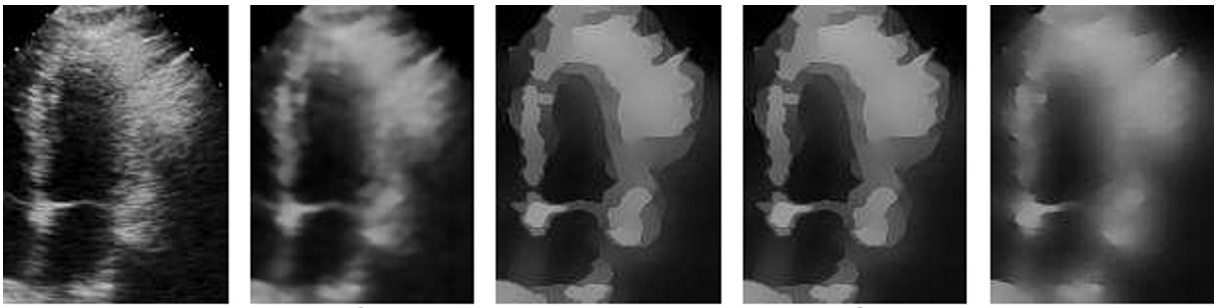

Fig. 1. Image processing results for several schemes and parameters.

$$\begin{cases} \dfrac{\partial u(x,y,t)}{\partial t} - c\Delta u(x,y,t) = f(x,y,t) \quad \text{everywhere in } \Omega \times [0,T], \\ u(x,y,t)_{|\partial\Omega} = 0, \quad \forall t \in [0,T] \quad \text{(boundary condition)}, \\ u(x,y,0) = u_0(x,y) \quad \text{(initial condition)}, \end{cases} \tag{16}$$

where, in this classical case the spatial discretization step size h is not fixed to one. If we consider the solution of problem (16) by an implicit scheme, then the condition number of each linear system to solve at each time step k, is obviously given by

$$\kappa^{(k)} = \frac{h^2 + 4c\tau(\sin(\frac{nm\pi h}{2}))^2}{h^2 + 4c\tau(\sin(\frac{\pi h}{2}))^2} \leqslant 1.0 + \frac{4c\tau}{h^2}\left(\sin\left(\frac{nm\pi h}{2}\right)\right)^2;$$

then

$$\kappa^{(k)} \leqslant 1.0 + \frac{4c\tau}{h^2} \to \infty \quad \text{if } h \to 0,$$

and in this case the condition number increases, on the contrary of the behavior arising in image processing where the spatial discretization step size h is fixed to one.

Remark 9. According to the notations of Remark 6, consider that $A^{(k)} = A_x^{(k)} + A_y^{(k)}$. Consider also that the spatial step size h_x and h_y are different in each direction x and y and are defined as in the previous Remark 6. α_x and α_y being defined in a similar way, then we can write

$$\kappa^{(k)} \leqslant \frac{\theta + \alpha_x(\lambda_x)_{\text{Max}} + \alpha_y(\lambda_y)_{\text{Max}}}{\theta + \alpha_x(\lambda_x)_{\text{min}} + \alpha_y(\lambda_y)_{\text{min}}},$$

where λ_x is one eigenvalue of $A_x^{(k)}$ and similarly for $A_y^{(k)}$. Then, $\frac{1}{\theta}$ being an upper bound of the inverse of the denominator, we obtain

$$\kappa^{(k)} \leqslant 1 + \frac{\alpha_x(\lambda_x)_{\text{Max}}}{\theta} + \frac{\alpha_y(\lambda_y)_{\text{Max}}}{\theta},$$

and since the diffusion coefficient is bounded by one, then

$$(\lambda_x)_{\text{Max}} \leqslant \left\|A_x^{(k)}\right\| \leqslant \max_{1\leqslant i\leqslant nm}\left(\sum_{j=1}^{nm}\left(\left|(a_x)_{i,j}\right|\right)\right) \leqslant 2(a_x)_{i,i} \leqslant 8,$$

and similarly for $(\lambda_y)_{\text{Max}} \leqslant 8$; then

$$\kappa^{(k)} \leqslant 1 + \frac{4\tau}{\theta}\left(\frac{(n+1)^2}{d^2} + \frac{(m+1)^2}{b^2}\right) = 1 + \frac{4\tau}{\theta}\left(\frac{1}{h_x^2} + \frac{1}{h_y^2}\right).$$

In fact, the numbers n and m are in the general case sufficiently large. So, from a numerical point of view only, we can see that h_x and h_y have small values. Nevertheless, in image processing, recall again that one considers that the parameters are non-dimensional such that $n+1 \simeq d$ and $m+1 \simeq b$, and, consequently the spatial discretization step size satisfies $h_x = h_y \approx 1$ (see [9] and [16]) and the upper bound of the condition number $\kappa^{(k)}, k \in \mathbb{N}$ is well given by (15) and, since τ is small, the upper bound of $\kappa^{(k)}, k \in \mathbb{N}$ is close to one.

Please cite this article in press as: C. Tauber et al., Iterative methods for anisotropic diffusion of speckled medical images, Applied Numerical Mathematics (2009), doi:10.1016/j.apnum.2009.11.002

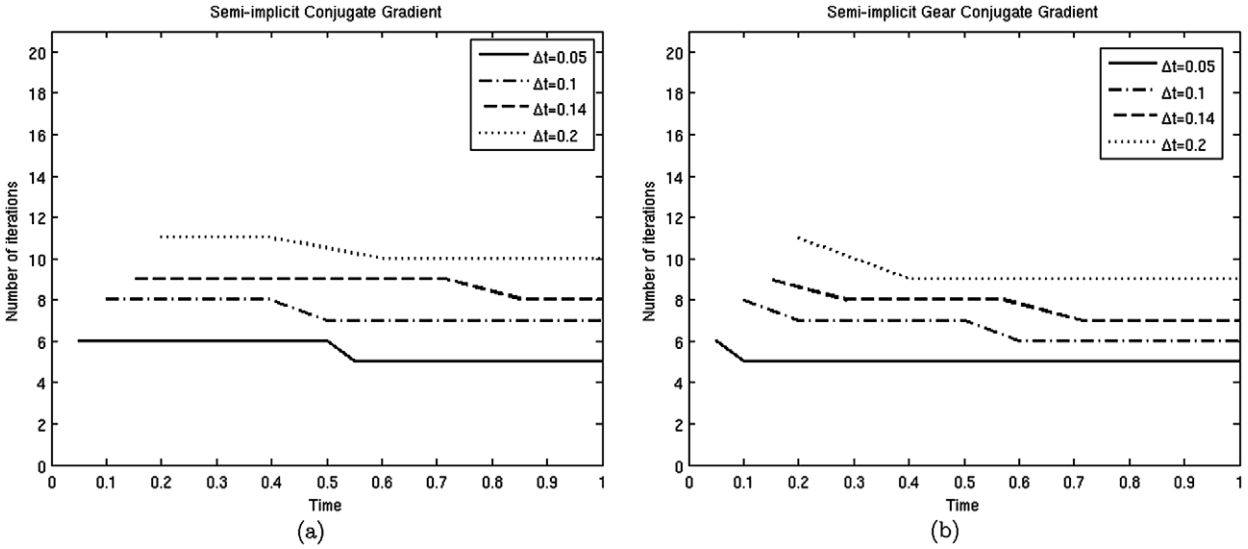

Fig. 2. Number of iterations with gradient conjugate method. (a) Semi-implicit scheme, (b) Gear semi-implicit scheme.

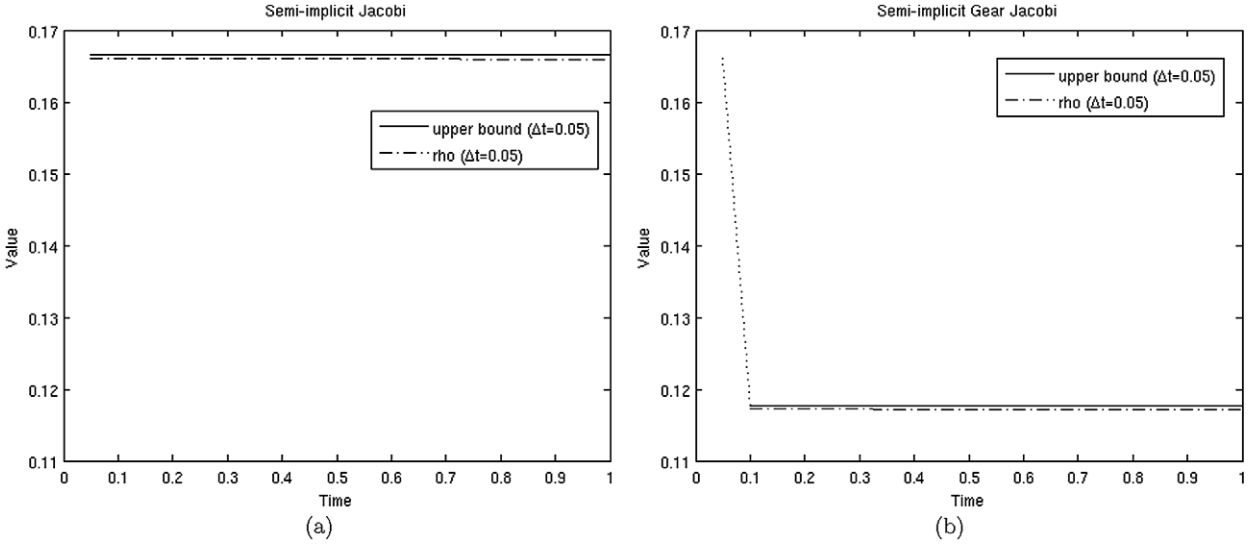

Fig. 3. Spectral radius of Jacobi matrix. (a) Semi-implicit scheme, (b) Gear semi-implicit scheme.

5. Numerical simulation results

Sequential numerical experiments have been performed on two kinds of ultrasound medical images. The first one called in the sequel image A has 116×154 pixels and the size of the system to solve is 17 328. It is an ultrasound image of the left ventricle and auricle of a human heart (see Fig. 1a). The second image is a synthetic ultrasound image called image B, that has 1024×1024 pixels, and leads to a system of size 1 044 484.

5.1. Image processing results

In ultrasound imaging, the information comes from two sources. The first one is the reflected signal. The ultrasound wave propagates through the tissues, until it encounters a change of density (an interface between two different organs for instance). The wave is then partially reflected, depending on the gradient of density. The signal that comes back (echo) is measured and used to reconstruct the image. The second source of information is ambiguous because it is both considered information and noise. This second source is the speckle. It originates from retro-diffusion causes by small diffractors that are disseminated within the tissues. These diffractors are small density changes that create small reflected signals that randomly walk within the tissue and eventually come back to the ultrasound probe. Speckle degrades the contrast but

Please cite this article in press as: C. Tauber et al., Iterative methods for anisotropic diffusion of speckled medical images, Applied Numerical Mathematics (2009), doi:10.1016/j.apnum.2009.11.002

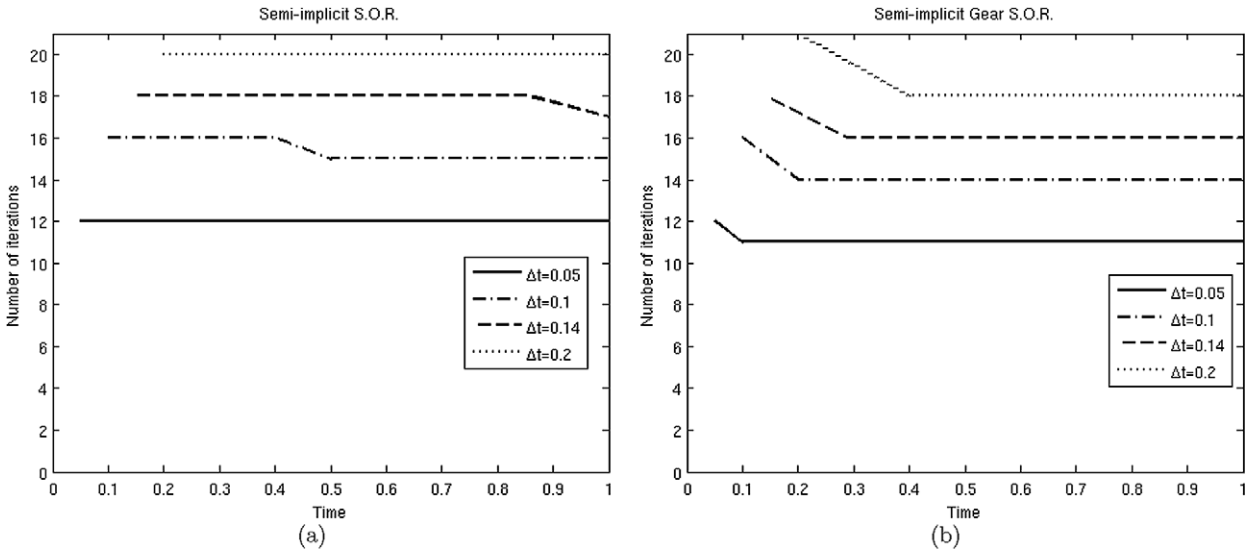

Fig. 4. Number of iterations with S.O.R. method. (a) Semi-implicit scheme, (b) Gear semi-implicit scheme.

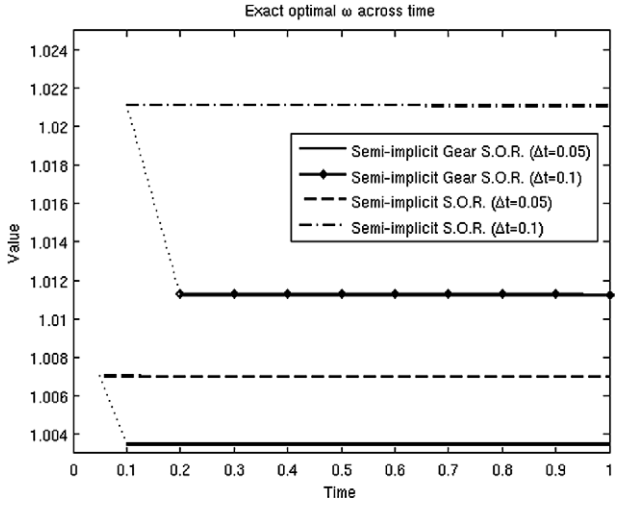

Fig. 5. Evolution of optimal relaxation value for semi-implicit scheme and Gear semi-implicit scheme.

also gives information on the local density of diffractors and their spatial organisation which differ for each organ. The anisotropic diffusion of the speckle has two objectives: reduce the variance of intensity in homogeneous regions, and recover a mean intensity that characterises each organ. The major difficulty is that because the speckle creates strong variance throughout the image, conventional edge detectors are ineffective. The coefficient of diffusion has thus to be specifically tailored to ensure robustness to speckle.

The global objectives enumerated in Section 1 were reached. Fig. 1a shows the original and speckled image. In particular the images presented in Figs. 1b, 1c and in 1d show that the processing reduces the variance in homogeneous regions and increases the contrast. Fig. 1b corresponds to a diffusion for one second with fifty time steps while Figs. 1c and 1d present the result after a diffusion of twenty five seconds with respectively twenty five and one thousand time steps. More precisely, we can note that the speckle is progressively reduced in homogeneous regions, while the boundaries between the different parts of the heart are more perceivable. Moreover, due to the modelization of the diffusion coefficient, infinite diffusion does not give uniform images, but instead tends to images similar to the ones obtained in Figs. 1c and 1d.

Finally, Fig. 1e corresponds to the same image processing filter using an instable explicit time marching scheme. It can be noted from Fig. 1c and from Fig. 1d that the semi-implicit scheme remains stable for time step $\tau = 1$ second, which is not the case for the explicit scheme (see Fig. 1e).

Please cite this article in press as: C. Tauber et al., Iterative methods for anisotropic diffusion of speckled medical images, Applied Numerical Mathematics (2009), doi:10.1016/j.apnum.2009.11.002

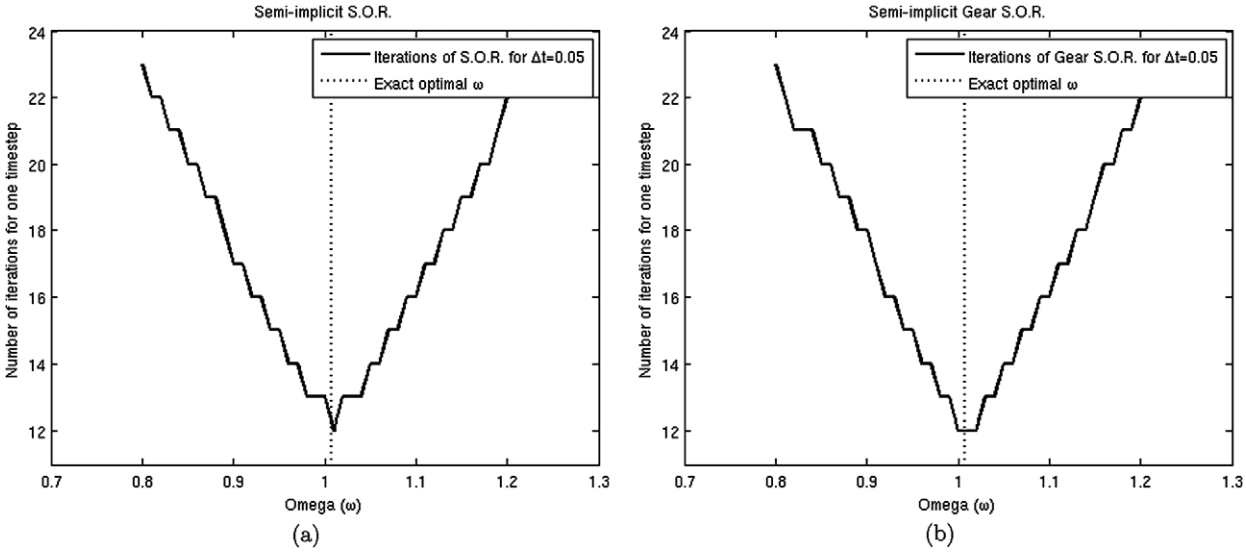

Fig. 6. Experimental value of optimal relaxation. (a) Semi-implicit scheme, (b) Gear semi-implicit scheme.

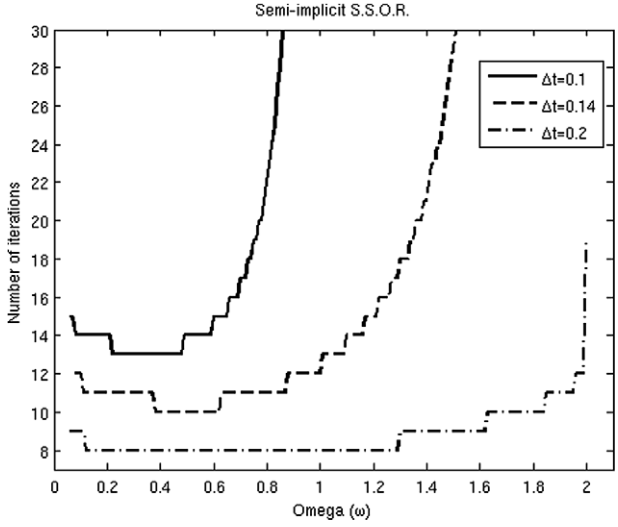

Fig. 7. Experimental values of optimal relaxation for S.S.O.R. preconditioning for semi-implicit scheme.

5.2. Results of sequential numerical experiments

Sequential simulations have been performed on a 2.4 GHz Apple Imac with processor Intel core 2 duo. The results of sequential experiments are summarized in Figs. 2 to 7 and in Tables 3 to 6.

For the two considered images, Tables 3 and 4 give the user CPU elapsed time for explicit scheme, semi-implicit scheme and Gear semi-implicit scheme, when the linear systems are solved by relaxation algorithms and conjugate gradient algorithm. In Fig. 2, note that the conjugate gradient method has the best rate of convergence; as a consequence this last method allows to obtain the lowest elapsed time for the iterative solution of the linear system at each time step $k \in \mathbb{N}$.

Nevertheless, the difference of performance between the compared iterative methods is not considerable. This is due to the fact that the cost of computation of the diffusion coefficient and of the entries of the matrix $A^{(k)}$ at each time step is important. When the conjugate gradient method is used, we can see that at each time step, the same time is necessary for solving the linear system, and for computing the diffusion coefficient and the entries of the matrix $A^{(k)}$. Moreover, in the case of using the semi-implicit scheme, and when the linear systems are solved by the optimized successive over-relaxation method, the total difference of elapsed time is about 12.80% greater than when we use the conjugate gradient algorithm. If we used the Gear semi-implicit scheme, the difference with the total of elapsed time is less (about 11, 23%); in this latter situation, the diagonal dominance of the matrix to inverse, i.e. $(\theta I + \alpha A^{(k)})$, is more important.

Please cite this article in press as: C. Tauber et al., Iterative methods for anisotropic diffusion of speckled medical images, Applied Numerical Mathematics (2009), doi:10.1016/j.apnum.2009.11.002

Table 3
C.P.U. time (sec.) for computation of image A.

τ	Explicit	Semi-implicit			Gear semi-implicit		
		Jacobi	S.O.R.	Conjugate	Jacobi	S.O.R.	Conjugate
$\frac{1}{5}$	0.139	0.246	0.200	0.187	0.231	0.192	0.183
$\frac{1}{7}$	0.157	0.281	0.281	0.217	0.263	0.224	0.211
$\frac{1}{10}$	0.186	0.331	0.280	0.257	0.309	0.268	0.251
$\frac{1}{20}$	0.283	0.488	0.425	0.390	0.458	0.412	0.384

Table 4
C.P.U. time (sec.) for computation of image B.

τ	Explicit	Semi-implicit			Gear semi-implicit		
		Jacobi	S.O.R.	Conjugate	Jacobi	S.O.R.	Conjugate
$\frac{1}{5}$	11.181	17.500	13.754	12.419	16.235	13.290	12.222
$\frac{1}{7}$	13.560	20.193	16.483	14.612	18.623	15.819	14.328
$\frac{1}{10}$	17.219	24.429	20.089	17.858	22.696	19.313	17.564
$\frac{1}{20}$	29.144	37.194	31.721	28.162	34.483	30.973	27.845

Table 5
Difference and corresponding percentage of elapsed time for optimized S.O.R. and conjugate gradient methods for image B.

τ	Semi-implicit method		Semi-implicit Gear method	
	Difference	Percentage	Difference	Percentage
$\frac{1}{5}$	1.335	10.75%	1.068	8.74%
$\frac{1}{7}$	1.871	12.80%	1.491	10.40%
$\frac{1}{10}$	2.231	12.49%	1.749	9.95%
$\frac{1}{20}$	3.559	12.63%	3.128	11.23%

Table 6
Percentage of zero rows for the matrix $A^{(k)}$ for image B during 10 time steps.

Time step n	Number of zero rows	Percentage of zero rows
1	3433	0.32%
2	4750	0.45%
3	6140	0.58%
4	7790	0.74%
5	9670	0.92%
6	11932	1.14%
7	14482	1.38%
8	17229	1.65%
9	19972	1.91%
10	22729	2.17%

For all used iterative methods, i.e. Jacobi, optimized S.O.R. and conjugate gradient methods, and for the two sizes of images considered, the computational times are low. Table 5 shows the difference in computational time and in percentage of the total computational time between the optimized S.O.R. and conjugate gradient methods.

For the explicit scheme, we obtain the best elapsed time; however, this scheme is unstable if τ is too large.

Table 6 shows in the case of semi-implicit scheme and for the image B, the number of zero rows in the matrix $A^{(k)}$, during the evolution process. At the first time step, 0.32% of the rows of the matrix $A^{(1)}$ are zero; at the last time step, when $k = 10$, 2.17% of the rows of the matrix $A^{(10)}$ are zero. Then, Table 6 shows clearly that the matrix $A^{(k)}, \forall k \in \mathbb{N}$, are reducible, this reducibility increases during the computational process.

Figs. 3a and 3b show the evolution of the spectral radius $\rho^{(k)}$ of the Jacobi matrix for both semi-implicit methods; the dashed line represents the exact value of $\rho^{(k)}$ computed during the evolution process using the power method while the solid line represents the evolution of an estimate of $\|\mathcal{J}^{(k)}\|_\infty$. It can be noted that, during the evolution process, $\rho^{(k)}$ is practically constant. Moreover the estimate of $\rho^{(k)}$ by $\|\mathcal{J}^{(k)}\|_\infty$ and the global upper bound (13) of $\rho^{(k)}$ are very accurate (see Table 1). Furthermore, since $\rho^{(k)}$ is slightly constant at each time step k, the same number of iterations of the Jacobi method is necessary for solving the linear systems at each time step; this has been observed by numerical experiments. As a consequence, since the spectral radius of the point Gauss–Seidel matrix is the square of the spectral radius of the Jacobi matrix, and since the optimal value of the optimal relaxation parameter is subordinated to the value of $\rho^{(k)}$, then at each time step, the same number of iterations of the point Gauss–Seidel method and of the point S.O.R method is necessary for

Please cite this article in press as: C. Tauber et al., Iterative methods for anisotropic diffusion of speckled medical images, Applied Numerical Mathematics (2009), doi:10.1016/j.apnum.2009.11.002

solving the linear systems. The same remark holds when using the conjugate gradient method to solve the linear systems in both semi-implicit schemes (see Fig. 4).

When the Gear semi-implicit scheme is used, it can be noted in Figs. 2b, 3b and 4b, that between the first time step and the second one, a discontinuity appears in the number of iterations during the evolution process. This discontinuity is due to the fact that for the first step of the Gear semi-implicit scheme, the semi-implicit scheme is used.

Figs. 6a and 6b show the influence of the value of the relaxation parameter on the number of iterations of the optimized S.O.R method at the first time step. We observe that we have the same behavior of the S.O.R optimized method for all time steps. It can be noted that the optimal value of the relaxation parameter is near one according to the estimate (15). Furthermore, during the time marching algorithm, Fig. 5 shows that, in accordance with the fact that during the evolution process the spectral radius of the Jacobi matrix is practically constant, the optimal value of the relaxation parameter is constant at each time step for both semi-implicit scheme and Gear semi-implicit scheme.

Finally, Fig. 7 shows that, in this particular application of image processing, the SSOR preconditioned conjugate gradient method does not improve the asymptotic rate of convergence of the conjugate gradient method (see [8] and [11]).

References

[1] L. Alvarez, P.L. Lions, J.M. Morel, Image selective smoothing and edge detection by nonlinear diffusion. II, SIAM J. Numer. Anal. 29 (3) (1992) 845–866.
[2] G. Aubert, P. Kornprobst, Mathematical Problems in Image Processing – Partial Differential Equations and the Calculus of Variations, second ed., Applied Mathematical Sciences, vol. 147, Springer, 2006.
[3] O. Axelson, Iterative Solution Methods, Cambridge University Press, 1996.
[4] M.J. Black, G. Sapiro, D.H. Marimont, D. Heeger, Robust anisotropic diffusion, IEEE Trans. Image Proc. 7 (3) (1998) 421–432.
[5] L. Blanc-Feraud, P. Charbonnier, G. Aubert, M. Barlaud, Nonlinear image processing: Modeling and fast algorithm for regularization with edge detection, Proc. Int. Conf. on Image Processing 1 (1995) 474–477.
[6] F. Catte, P.L. Lions, J.M. Morel, T. Coll, Image selective smoothing and edge detection by nonlinear diffusion, SIAM J. Numer. Anal. 29 (1) (1992) 182–193.
[7] R. Dautray, J.L. Lions, Analyse mathématique et calcul numérique pour les sciences et les techniques, tome 9, Masson, 1988.
[8] J.C. Miellou, P. Spiteri, Optimization of the relaxation parameter for S.S.O.R. and A.D.I. preconditioning, Numer. Algorithm 29 (2002) 155–195.
[9] P. Perona, J. Malik, Scale-space and edge detection using anisotropic diffusion, IEEE Trans. Pattern Anal. Machine Intell. 12 (7) (1990) 629–639.
[10] P.J. Rousseeuw, A.M. Leroy, Regression and Outlier Detection, Wiley, New York, 1987.
[11] P. Spiteri, J.C. Miellou, J. Bahi, Evaluations of parameters for the optimization of S.S.O.R. and A.D.I. preconditioning, Numer. Algorithm 29 (2002) 249–265.
[12] C. Tauber, H. Batatia, A. Ayache, A robust speckle reducing anisotropic diffusion, IEEE ICIP 1 (2004) 247–250.
[13] J.W. Tukey, Exploratory Data Analysis, Addison-Wesley, Reading, MA, 1977.
[14] R.S. Varga, Matrix Iterative Analysis, second ed., Prentice-Hall, Inc, 1962 and Series in Computational Mathematics, Springer, 2000.
[15] J. Weickert, B.M. Haar Romeny, M.A. Viergever, Efficient and reliable schemes for nonlinear diffusion filtering, IEEE Trans. Image Proc. 7 (3) (1998) 398–410.
[16] J. Weickert, Anisotropic diffusion in image processing, Ph.D. thesis, Dept. of Mathematics, University of Kaiserslautern, Germany, 1996.
[17] Y. Yu, S.T. Acton, Speckle reducing anisotropic diffusion, IEEE Trans. Image Proc. 11 (11) (2002) 1260–1270.

Please cite this article in press as: C. Tauber et al., Iterative methods for anisotropic diffusion of speckled medical images, Applied Numerical Mathematics (2009), doi:10.1016/j.apnum.2009.11.002